

# Extending the hydrodynamical description of heavy-ion collisions to the “outer edge” of the fireball

Adith Ramamurti\* and Edward Shuryak†

*Department of Physics and Astronomy,  
Stony Brook University,  
Stony Brook, NY 11794, USA  
(Dated: January 12, 2022)*

It is well known that relativistic hydrodynamics provides very good description of heavy-ion collisions at RHIC/LHC energies up to transverse momenta  $p_{\perp} \sim 2$  GeV. In this paper, we suggest that this description can be extended to higher  $p_{\perp} \sim 6$  GeV, beyond which hard collisions contribute. While most previous work focused on a part of the freezeout surface at the latest proper time (referred to in this work as the “lid”), we focus on the complementary part, to be referred as “the outer edge,” where the highest transverse rapidity of flow  $\kappa \sim 1.4$  is achieved. We study this surface analytically, using the Riemann rarefaction wave, and numerically, using MUSIC numerical hydrodynamic code. We also use an improved freezeout condition, where the collision rate equals the expansion rate. For central collisions, we observe good description of spectra for  $\pi, K, N$  in central PbPb LHC collisions in this extended region. We further suggest that “the outer edge” has very small azimuthal asymmetry even for non-central collisions, smaller than predicted by standard hydrodynamics.

## I. INTRODUCTION

It is by now established that high energy heavy-ion collisions, and even high-multiplicity  $pA$  and  $pp$  collisions, can be rather well described by relativistic hydrodynamics; for reviews see Refs. [1–4]. These hydrodynamical descriptions of spectra are typically accepted from small transverse momenta up to  $p_{\perp} \sim 2$  GeV. The reasons given for this upper limit differ from paper to paper, and can be summarized as follows:

- (i) the afterburner cascade runs out of statistics;
- (ii) the viscous corrections to thermal distribution in the hydro cell may become large [5];
- (iii) above  $p_{\perp} > 2 - 3$  GeV the azimuthal harmonic flows  $v_n(p_{\perp})$  no longer follow the characteristic hydro-based linear regime  $v_n(p_{\perp}) \sim p_{\perp}$ .

As we will show, the spectra change shape and produce evidence for hard collisions and

jet-related phenomena several orders lower, at  $p_{\perp}^{\max} \sim 5 - 6$  GeV. At present, there exists no generally agreed explanation for the origin of secondaries in the intermediate region of transverse momenta  $2 \text{ GeV} < p_{\perp} < p_{\perp}^{\max}$ .

The only previous attempt to explain spectra in this region, by a coalescence of jet-related and hydro-related quarks [6], predicted a certain “quark scaling” of elliptic flow. Not going into its criticism, let us just note that our proposal is completely different. In particular, we discuss secondaries coming from the freezeout surface at proper time  $\tau \sim 20$  fm/c, whereas all jets leave the fireball much earlier, at  $\tau < 6$  fm/c, so no coalescence is possible.

Standard application of – by now, rather sophisticated – hydrodynamics is usually supplemented by very crude treatment of the final stage of the process, known as the freezeout. The spectra are calculated by calculating Cooper-Frye integral over a certain surface, which in practice is taken to be an isotherm with a particular temperature  $T_f$ .

One of the improvements we try to develop in this work is to substitute the isotherm by another surface, prescribed by a more meaningful freezeout condition relating the expansion rate of matter to the corresponding reaction rates.

As we will show below, the freezeout surface (FOS) consists of two distinct parts. One of

\* [adith.ramamurti@stonybrook.edu](mailto:adith.ramamurti@stonybrook.edu)

† [edward.shuryak@stonybrook.edu](mailto:edward.shuryak@stonybrook.edu)

them, to be called the “lid,” is characterized by a Hubble-like flow, with transverse rapidity growing approximately linearly with the radial distance from the center,  $\kappa \sim r$ . This part dominates spectra at not-too-large  $p_{\perp}$ , and was studied extensively, e.g. with the so-called “blast wave” parameterizations. While our work somewhat modified the FOS itself, the spectra at  $p_{\perp} < 2$  GeV remain unchanged as compared to multiple previous works.

The part of the FOS we will discuss in this work is the “outer edge.” We will show that at larger  $p_{\perp}$ , its contribution to the spectra becomes dominant. Indeed, in this region spectra are very sensitive to the maximal value of transverse collective flow, and the “outer edge” generates transverse rapidity up to  $\kappa \sim 1.4$  exceeding that of the “lid”  $\kappa < 1.2$ .

We will work out an analytic solution, approximating this region, based on the Riemann “rarefaction fan” solution, and compare it with the standard numerical solution of hydrodynamics. We will further show that  $T$  and  $u^{\mu}$  in this region are indeed directly related to each other.

We will also reformulate the freezeout condition itself, incorporating local information on the matter expansion rate  $\partial_{\mu}u^{\mu}$ . Since even in the case of the rarefaction fan, this quantity is *not* constant on the isotherm, we have to conclude that the correct FOS *cannot* be an isotherm. We will then show how the FOS gets modified.

Accounting for all of this, we see rather encouraging description of particle spectra for a greater range of  $p_{\perp}$ . It is important to stress that this applies for secondaries of different masses, such as  $\pi$ ,  $K$ ,  $N$ .

In this paper, we will only discuss central collisions and axially symmetric flow. A paper to follow will deal with non-central collisions and elliptic flow.

## II. MOTIVATION

### A. The extent of thermal mass spectra at the chemical freezeout

A fireball created in heavy-ion collisions is generally considered to be a “well-equilibrated”

thermal system, at least by its freezeout stages. A more precise meaning of this statement comes from comparison of the mass distributions of the secondaries with the Boltzmann exponent, corresponding to chemical freezeout temperature  $T_{\text{ch}} \approx 156$  MeV (and baryonic chemical potential  $\mu_b$ ). An example of such a comparison is replicated in Fig. 1, from Ref. [7]. As one can see, the thermal description correctly reproduces the observed particle yields for about nine orders of magnitude.

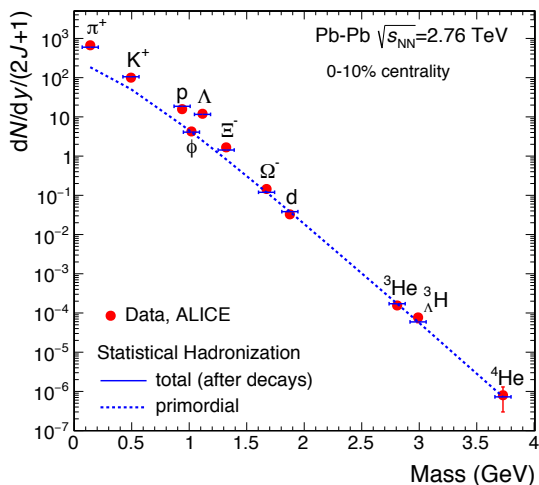


FIG. 1. with the statistical weights removed, plotted as a function of the particle mass. The horizontal blue lines are with the decays of the resonances, the dotted blue line are primordial only. From Ref. [7].

In this paper, we discuss not the mass but energy and momenta distributions. Those are determined at the kinetic freezeout stage, corresponding to somewhat later times as compared to chemical freezeout, with lower temperature  $T_f \approx 100$  MeV as compared to  $T_{\text{ch}} \approx 156$  MeV. It is widely expected that collisions happening in a hadronic resonance gas, between these two freezeout temperatures, does not spoil the thermal equilibration.

Of course, particle masses are Lorentz scalars, and their distribution is unaffected by motion of matter, while the particle energies and momenta are components of Lorentz vector and are affected by it. Unlike the total par-

ticle yields, calculation of the observed spectra requires a precise knowledge of the flow velocity on the freezeout surface. But, with relatively small flow gradients at late stages of the collision, one may still think that thermal distribution is reasonably well maintained in each hydro cell. Optimistically, we therefore assume that with some distribution of the flow, either obtained from some phenomenological model or from numerical hydrodynamics, one may be able to describe the particle spectra over a similar range of  $p_{\perp}$ , or to energies (in co-moving frame) of a similar magnitude as the masses, or not less than 4 GeV.

## B. Looking for changes in the observed $p_{\perp}$ spectra

Since we focus on large  $m_{\perp}, p_{\perp} \gg T$  part of the spectrum in this work, the arguments of the Bessel functions in Eq. A2 are large, and one can approximate them by the exponent with a “blue shifted slope”  $\hat{T} = Te^{\kappa}$ ,

$$\exp\left[-\frac{p_{\perp}}{T}(\cosh(\kappa) - \sinh(\kappa))\right] = \exp\left[-\frac{p_{\perp}}{\hat{T}}\right]. \quad (1)$$

Let us now have a look at the effective temperature extracted from the observed spectra, defined as its logarithmic derivative. This quantity is plotted in Fig. 2 as a function of transverse rapidity  $y_{\perp} = \text{arcsinh}[p_{\perp}/m]$ . As one can observe from this plot, the slope grows very gradually, till a value of  $y_{\perp} \sim 4.2$  (corresponding to pion momenta  $p_{\perp} > 5 \text{ GeV}/c$ ). At higher transverse rapidities, the slope changes and starts to grow more rapidly. Similar changes of spectra are observed for other secondaries, at different rapidities but similar  $p_{\perp}$ . This change of spectra, from near-exponential to power-like, is a well-known phenomenon induced by hard partonic processes related to jet production. In summary, spectra themselves also suggest that perhaps the limits of thermal description should be somewhere at  $p_{\perp} \sim 5 \text{ GeV}/c$ , in the same ballpark as the thermal distributions over masses.

Now, how can pions reach transverse rapidity as large as  $y_{\perp}^{\text{max}} \sim 4$ ? What fraction of them are from thermal and what from collective motion? From multiple studies of spectra at small

$p_{\perp}$ , we know that for central PbPb LHC collisions the value of kinetic freezeout temperature is rather low,  $T_f \approx 0.1 \text{ GeV}$ . Comparing it to the effective “blue shifted” slope  $\hat{T} \approx 0.4 \text{ GeV}$  of Fig. 2, one may conclude that some parts of the FOS must have the “blue-shift” factor  $\exp(\kappa_{\text{max}}) \sim 4$ , corresponding to the transverse rapidity of the flow

$$\kappa_{\text{max}} \approx 1.5 \quad (2)$$

(The corresponding rapidity of the thermal motion in the matter frame should then be  $y_{\perp} - \kappa_{\text{max}} \approx 2.5$ , the energy in the matter rest frame  $E_{\pi} = m_{\pi} \cosh(2.5) \approx 0.85 \text{ GeV}$ , and the Boltzmann factor  $\exp(-E_{\pi}i/T_f) \sim 2 \times 10^{-4}$ , more than an order of magnitude above the fraction of the transverse momentum spectrum at the discussed  $p_{\perp}$  of  $\sim 10^{-5}$ .)

One of the main points of this paper, is that the “outer edge” of the fireball can in fact deliver a transverse collective flow of this magnitude.

The questions we will be discussing below are then:

- (i) Can the collective flow with the transverse rapidity as large as  $\kappa \sim \kappa_{\text{max}}$  be phenomenologically acceptable, providing consistent description of spectra for species of secondaries of very different mass?
- (ii) Can a flow with a transverse rapidity as large as  $\kappa \sim \kappa_{\text{max}}$  be generated hydrodynamically?
- (iii) Where would this region of the fireball be located? Can it be analytically understood?

We will argue that all of them can be answered in the affirmative.

## III. USING ANALYTIC SOLUTIONS OF RELATIVISTIC HYDRODYNAMICS

### A. Gubser flow

While mainstream development of these ideas relied mostly on numerical codes, without and with viscosity terms, one cannot overestimate the value of analytic solutions, ranging from the original Landau solution [8], the

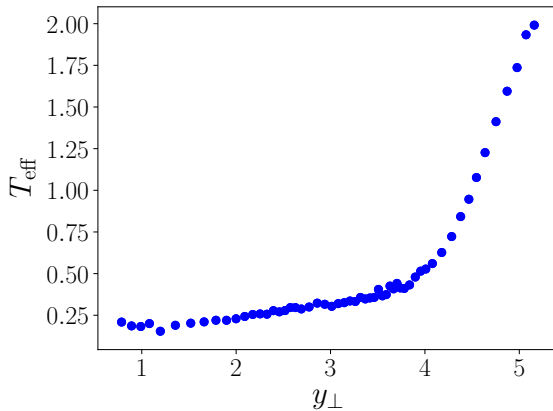


FIG. 2. The effective temperature defined as the logarithmic derivative of the  $p_{\perp}$  distribution, as a function of transverse rapidity  $y_{\perp}$ .

Bjorken rapidity independent 1+1 dimensional solution [9] and the Gubser solution [10, 11], which makes use of scale invariance of quark-gluon plasma (QGP) and is obtained by a conformal transformation.

Apart of pedagogical value, and that of code verification, analytic solutions allow us to reach understanding and derive results, which would otherwise take a much longer time. For example, using small perturbation on top of Gubser flow, P. Staig and one of us [12] found a complete Green function – expanding deformed sound sphere from a delta-function-like source in the initial conditions –, which predicted a very non-trivial shape of two-particle correlation function in azimuthal angle, soon confirmed by experiment. Gubser flow has also been used for calculation of the radial flow [13] and femtoscopy radii [14] in “small systems,” the high-multiplicity  $pp, pA$  collisions.

These studies, however, have revealed that the Gubser solution can resemble real heavy-ion collisions, and thus be useful, only for the “lid” portion of the freezeout surface. This is because of its relatively slow (power-like) decrease of the densities with distance, which do not correspond to actual fireballs. One may explain it as follows: Gubser’s fireball expands not in vacuum, but into some kind of atmosphere, which prevents the necessary flow development at the outer edge.

Looking for solutions independent on both “angles”  $\eta, \phi$  out of four coordinates, Gubser’s solution is

$$u_{\mu} = (-\cosh \kappa(\tau, r), 0, \sinh \kappa(\tau, r), 0) \quad (3)$$

Gubser obtained the following solution

$$v_{\perp} = \tanh \kappa(\tau, r) = \left( \frac{2q^2\tau r}{1 + q^2\tau^2 + q^2r^2} \right) \quad (4)$$

$$\epsilon = \frac{\hat{\epsilon}_0(2q)^{8/3}}{\tau^{4/3}(1 + 2q^2(\tau^2 + r^2) + q^4(\tau^2 - r^2)^2)^{4/3}}$$

The solution has two parameters,  $\hat{\epsilon}_0$  and  $q$ , representing the scale of the energy density and the size of the fireball, respectively.

Requiring the freezeout surface to be the isotherm  $\epsilon(\tau, r) = \epsilon_f$  one can find  $\tau_f(r)$ , and, substituting it into the collective velocity/rapidity, find its distribution on the surface. An example of such procedure is shown in Fig.3.

The linear growth from  $r = 0$  corresponds to the “lid” part of the freezeout surface. At the peak of this distribution the value of the transverse flow rapidity  $\kappa$  may be tuned to a phenomenological value needed to describe the data,  $\kappa_{\max}$ , yet it does so only at the thin “rim” of the fireball. At larger  $r$ , one finds that the flow rapidity *decreases* with distance. We will argue that this behavior is wrong, as it is inconsistent with the trend expected from universal properties of “rarefaction fan” portion of the solution and actual numerical solutions. This fact has been emphasized already in Ref. [12], and traced to the unphysically slow (power-like) decrease of the initial matter distribution. (To give the idea of what such slow tail means, compare it to an explosion in the atmosphere, which stops the flow at certain distance.) Therefore, spectra were calculated in Ref. [12] using only the late-time part of the freezeout surface.

For the record, one can calculate the expansion rate for Gubser flow, and find it to be (in  $q = 1$  units)

$$\partial_{\mu} u^{\mu} = \frac{4\tau}{\sqrt{(1 + r^2 + \tau^2)^2 - 4r^2\tau^2}} \quad (5)$$

Using it, one can plot the surfaces corresponding to the freezeout condition.

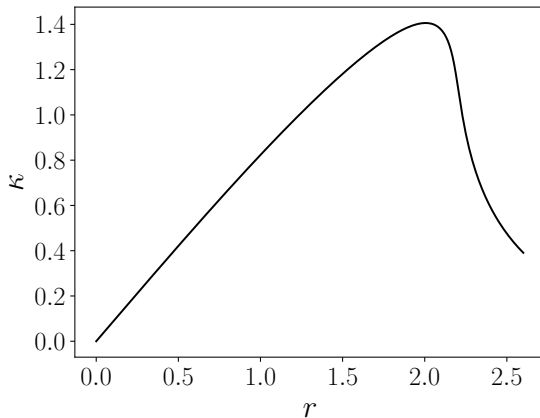


FIG. 3. The value of the transverse flow rapidity  $\kappa$  versus the radial distance  $r$  (in  $1/q$  units) at the freezeout isotherm for Gubser flow.

#### IV. THE RAREFACTION FAN

The solution we discuss is, in principle, known; in the fully-relativistic 1+1d context, it was first discussed in Ref. [15]. However, at that time, the magnitude of the flow was expected to be very small: e.g. in that paper, pions with  $p_{\perp} \sim 30$  MeV were considered, which is about hundred times (!) smaller than what we are going to discuss below. We will also rederive the solution, in pedagogically simpler way.

The main simplification, leading to the expansion solution we will discuss, is due to Riemann, who assumed that in the rarefaction fan region, the two unknown functions, e.g. the energy density  $\epsilon(\tau, x)$  and flow rapidity  $y(\tau, x)$ , are *not* independent but in fact are directly related to each other, namely

$$\epsilon(\tau, x) = f(y(\tau, x)). \quad (6)$$

Therefore, the isotherms, which are not exactly the FOS but close to it, and  $y(\tau, x) = \text{const.}$  are the *same lines* in this region! This property has

the historic name of ‘‘Riemann simple wave.’’ (In fact, many numerical solvers for astrophysical relativistic hydro are based on application of it at each space cell and each time step.)

Now is perhaps the time to revisit its usage, applying it now to where it belongs, the large-momentum tail of the particle spectra. Here, for pedagogical reasons, we give explicit solution of the rarefaction fan directly from the equations, without use of a Riemann invariant.

For 1+1 dimensional relativistic hydrodynamics, we will not change coordinates, keeping the original  $t, x$  coordinates. Using standard rapidity notations for 4-velocity,

$$u^0 = \cosh(y), \quad u^1 = \sinh(y), \quad (7)$$

one has the stress tensor in the form

$$T^{00} = \epsilon \cosh^2(y) + p \sinh^2(y), \quad (8)$$

$$T^{01} = (\epsilon + p) \cosh(y) \sinh(y), \quad (9)$$

$$T^{11} = \epsilon \sinh^2(y) + p \cosh^2(y), \quad (10)$$

subject to two equations

$$\frac{\partial T^{00}}{\partial t} + \frac{\partial T^{01}}{\partial x} = 0, \quad (11)$$

$$\frac{\partial T^{01}}{\partial t} + \frac{\partial T^{11}}{\partial x} = 0. \quad (12)$$

For simplicity, we will use EOS  $p = c_s^2 \epsilon$  with constant speed of sound  $c_s$ .

The first step toward solving the above is the Riemann idea to look for a solution in which all unknown functions are directly related to each other, in our case

$$\epsilon(t, x) = F(y(t, x)). \quad (13)$$

The second idea is that, since the EOS used has no dimensional parameters, the solution is perhaps self-similar

$$y(t, x) = f\left(\frac{t}{x}\right). \quad (14)$$

---

Substituting those to the equations of motion (Eq. 8) one have them in the form

$$\frac{F'(f)}{F(f)} + \frac{-2(1 + c_s^2)(t \cosh(2f) - x \sinh(2f))}{x - c_s^2 x + (1 + c_s^2)x \cosh(2f) - (1 + c_s^2)t \sinh(2f)} = 0,$$

$$\frac{F'(f)}{F(f)} + \frac{2(1+c_s^2)(x \cosh(2f) - t \sinh(2f))}{t - c_s^2 t - (1+c_s^2)t \cosh(2f) + (1+c_s^2)x \sinh(2f)} = 0.$$

The key consequence of the Riemann assumption is that the derivative  $f'$  appears in all terms and, if nonzero, can be cancelled out. As a result, one can find  $f$  from the ordinary (not a differential) equation, requiring two complicated ratios in the two EOM to be equal to each other. This relatively complicated equation leads to a surprisingly simple answer,

$$y = f(t/x) = \frac{1}{2} \log \left[ \left( \frac{1-c_s}{1+c_s} \right) \left( \frac{t+x}{t-x} \right) \right]. \quad (15)$$

Note that the logarithm in the second bracket corresponds to the so-called spatial rapidity

$$\eta(t, x) = \frac{1}{2} \log \left( \frac{t+x}{t-x} \right). \quad (16)$$

Substituting it into these ratios, one finds that both are indeed the same and the remaining equation takes the form

$$\frac{1+c_s^2}{c_s} + \frac{F'(f)}{F(f)} = 0,$$

from which

$$F(f) = \exp \left[ - \left( \frac{1+c_s^2}{c_s} \right) f \right].$$

times an arbitrary constant, to be determined from the boundary conditions.

For discussion to follow, we will need the scalar expansion rate, so let us give it for this flow

$$\partial_\mu u^\mu = \frac{1}{\sqrt{(1-c_s^2)(t^2-x^2)}}, \quad (17)$$

which is, as expected, Lorentz invariant.

## V. THE “CONICAL CUP” MODEL

After discussion of the Gubser solution, we would like to introduce a simple model which has properties much closer to what realistic hydrodynamical explosion predicts.

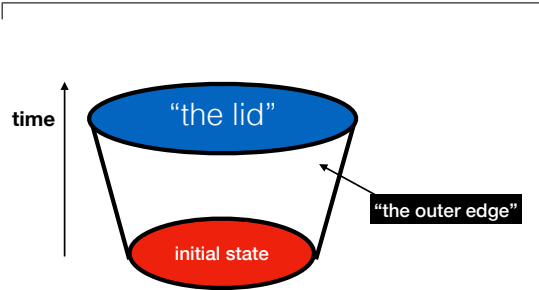


FIG. 4. Schematic picture of the freezeout surface in coordinates  $r$ -proper time  $\tau$ .

The schematic shape, we call the “conical cup”, is shown in Fig.5. It consists of the “top” part, taken to be at constant (longitudinal) proper time  $\tau = \tau_f$ , and the “outer edge”, taken to be of conical shape, with radius linearly interpolating between the initial and final radii,  $R_i$  and  $R_f$ . The bottom part is where the initial conditions are to be defined; it is understood to be at small but finite proper time  $\tau_i$  where one can start hydrodynamical description. We will not discuss the bottom part in this paper anymore, and the time  $\tau_i$ , typically a fraction of fm/c, is simply neglected compared to  $\tau_f \sim 17$  fm/c. For justification of the model and realistic values of its parameters, the reader should wait for later sections.

We further assume that at the top part of the surface the transverse rapidity dependence on  $r$  is linear, up to its maximal value

$$\kappa(r) = \kappa_{\max} \frac{r}{R_f}, \quad (r < R_f) \quad (18)$$

Note that because  $\tau = \text{const.}$  on the top part, the second term in the preceding expression vanishes.

On the outer edge, we assume that the transverse rapidity takes the same value on the whole wall,  $\kappa = \kappa_{\text{wall}}$ . (Justification to follow later.) If so, the Bessel functions decouple from the integral over the wall, up to the volume factor

$$V_{\text{wall}} = \int_0^{\tau_f} d\tau \pi R_\tau^2. \quad (19)$$

As we will show later, only a part of the wall actually corresponds to the solution with the constant (the highest)  $\kappa = \kappa_{\max}$ , so we introduce additional factor  $P_{\text{wall}}$  to the outer edge

contribution. Note also, that in this case the two terms with different Bessel functions compete.

The resulting spectra for this model are shown in Fig. 5, for the pions and protons. The previous studies focused on the “lid” contribution, shown by dash-dotted lines, which provides good description of the shape of the distribution up to  $p_{\perp} \sim 3 \text{ GeV}$ . Note further, that the excess seen in the data at small  $p_{\perp}$  is due to the so-called “feed-down” contribution, that of the decay of multiple mesonic and baryonic resonances. It is well known and calculated in statistical hadronization models, such as Ref. [7].

The new contribution of the “outer edge” we introduced now, shown by the solid lines, is small in the integral, of the order of a percent. However it becomes dominant at higher transverse momenta, improving agreement for pions for  $p_{\perp} = 2 - 5 \text{ GeV}$  and for protons for  $p_{\perp} = 3 - 6 \text{ GeV}$ . It significantly extends the description of the spectra in terms of absolute probability, by 2-3 orders of magnitude. This is important, because it now extends right up to the momenta  $p_{\perp} > 5 - 6 \text{ GeV}$  where the contribution from hard partonic reactions, eliminating the “nobody’s land” region in between.

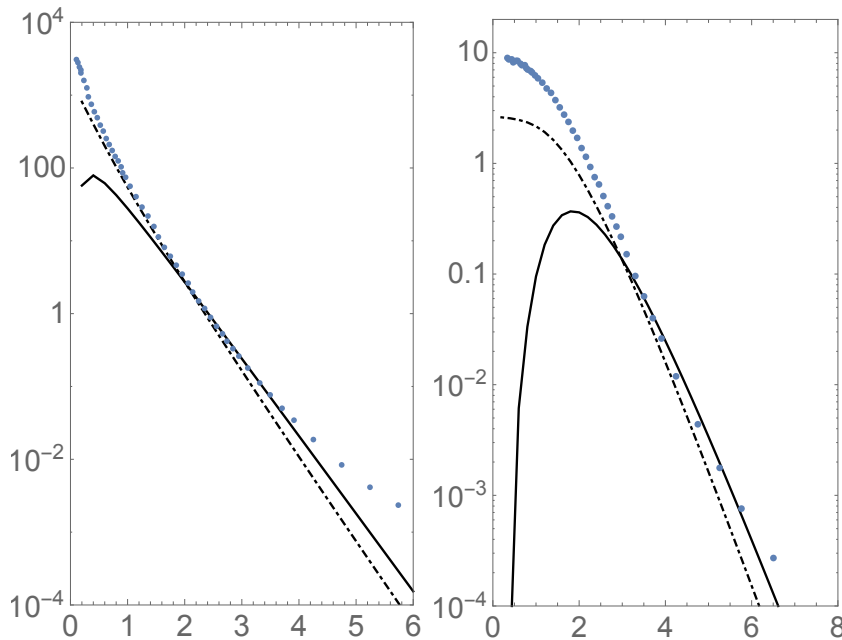


FIG. 5. The transverse momentum spectrum  $dN/dydp_{\perp}^2 ((\text{GeV}/c)^{-2})$  versus transverse momentum  $p_{\perp} (\text{GeV}/c)$  for pions (the left plot) and protons (the right plot). The points correspond to ALICE 0-5% centrality data from Ref. [16], the dash-dotted lines show the “lid” contribution, and the solid lines show that of the “outer edge,” with additional factor  $P_{\text{edge}} = 1/4$ .

## VI. TRANSVERSE FLOW AT THE ISOTHERM SURFACES OF NUMERICAL HYDRODYNAMICS

As input, we use an ensemble of hydrodynamic solutions generated from Glauber-based

initial conditions by the MUSIC [17]. We use smooth (Glauber-based) initial conditions and

take small impact parameter, corresponding to 0-5% centrality bin, the same as in the ALICE data [16] to which we will be comparing our results.

In the upper Fig. 6 we show location of the points at the isotherm  $T = T_f = 100 \text{ MeV}$ , on the  $r - \tau$  plane. Their distribution clearly display two parts of the f.o. surface: (i) the “lid;” and (ii) the “outer edge;” discussed above. The slope of the edge tells us that it moves outward with the velocity  $v_{\text{edge}} \approx 1/3$  (not to be confused with the collective flow velocity on this edge, which is much larger).

In the lower plot of Fig. 6, we show the corresponding distribution of the transverse flow rapidity  $\kappa(r)$ . It consists of a familiar Hubble-like linear rise on the “lid” part of the FOS, complemented by an upper “loop,” generated at the “outer edge”. This plot is to be contrasted with Fig. 3 for the Gubser flow, in which such a “loop” is absent. The main observation here is that the “loop” indeed reaches the maximal transverse rapidity value (Eq. 2) discussed above, required to describe the high- $p_{\perp}$  spectra.

## VII. THE IMPROVED FREEZEOUT CONDITION AND FOS'S

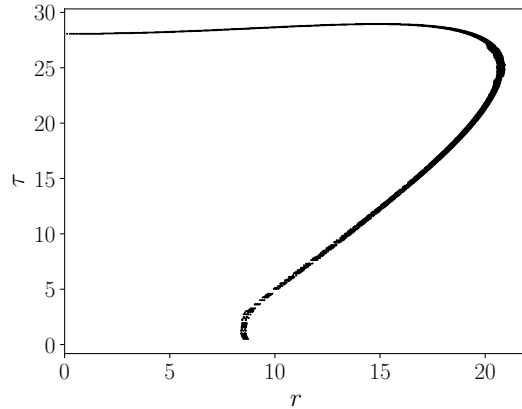
For high energy collisions, the idea of freeze-out [18] predated even the first application of relativistic hydrodynamics by Landau. It is also widely used in Big Bang cosmology. Schematically, the condition reads

$$\text{collision rate} = \text{expansion rate}$$

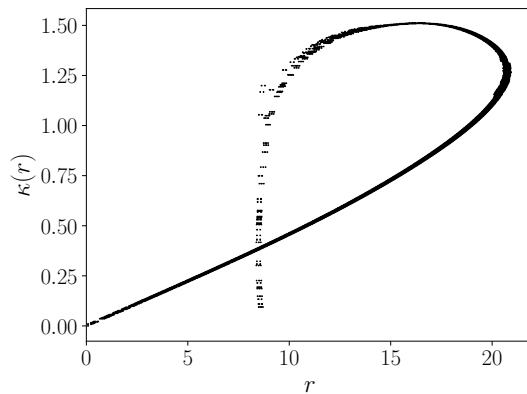
A more precise form used in Ref. [19] is, for the particle of type  $i$

$$\dot{w}_i = \langle \sum_j n_j \sigma_{ij} v_{ij} \rangle \approx \partial_{\mu} u^{\mu}, \quad (20)$$

where in the l.h.s. the sum is taken over all particle types  $j$ , with mutual scattering cross section and relative velocity. Note that the collision rates in the l.h.s. depend on  $i$ ; the freeze-out surface is not the same for different particle types. For example, the nucleons have large  $\sigma_{\pi N} \approx 200 \text{ mb}$  at the  $\Delta$  peak, and thus they are expected to decouple *later* than the pions. Strange particles such as  $\phi$  have smaller cross



(a)



(b)

FIG. 6. The upper plot (a) shows the freezeout surface  $T = 100 \text{ MeV}$ , in  $r, \tau(\text{fm})$  coordinates. The lower plot (b) shows the transverse flow rapidity  $\kappa(r)$  versus the radial distance  $r(\text{fm})$ . The dots represent hydro cells at the freezeout surface, corresponding to numerical solution using MUSIC code for 0-5% centrality.

sections, and thus should decouple *earlier* than the pions, etc.

Although these considerations and the collision rates in hadronic gas are well known, we have not seen them being used often, since that early paper [19].

The rates generally grow rapidly with the temperature  $T$ , and can be conveniently parameterized in a power form

$$\dot{w}_i = C_i T^{P_i}. \quad (21)$$



For example, in a cool gas of pions described by the Weinberg chiral Lagrangian, one finds  $\dot{w}_\pi \sim T^5/f_\pi^4$ . Taking the root of the power  $P_i$  and rewriting the freezeout condition back for  $T$ , one can put it in the following convenient form

$$T(x) = \left[ \frac{\partial_\mu u^\mu(x)}{C_i} \right]^{1/P_i}. \quad (22)$$

So, when the power  $P_i$  is very large, the r.h.s. is nearly constant, and thus the f.o. surface reduces back to the isotherm. However, the realistic power is  $P \approx 3.5$ , and in general both  $T(x^\mu)$  and  $\partial_\mu u^\mu(x^\nu)$  are some nontrivial functions of the space-time coordinates, obtainable from hydro equations.

Before presenting the results of the numerical hydrodynamics, let us now analyze the space-time distribution of expansion rate, starting from the “lid”, and then proceeding to the “outer edge”.

Taking the “lid” at fixed proper time and taking, for simplicity, the non-relativistic part of it, one can express linear rapidity growth with  $r$  as a “Hubble flow”

$$v_r = Hr \quad (23)$$

The divergence of this, in spherical coordinates, is

$$\partial_m u^m \approx \frac{1}{r^2} \frac{\partial}{\partial r} (r^2 v_r) = 3H, \quad (24)$$

which is a constant. Its magnitude is readily obtained; from the slope of the rapidity plot, one finds that  $H \approx 1/(20 \text{ fm})$  from which  $(1/\tau_{\text{exp}}) = 3H \approx (1/7 \text{ fm})$ . This value agrees well with the pion collision rate  $1/\tau_{\text{coll}}(T = 100 \text{ MeV})$  from Ref. [19].

On the “outer edge,” a similar estimate goes as follows. In this case, one should use cylindrical coordinates, so the expansion rate is

$$\frac{\partial}{\partial \tau} \cosh(\kappa) + \frac{1}{r} \frac{\partial}{\partial r} (r \sinh(\kappa)) \quad (25)$$

It is simple to calculate it at the isotherm, since according to rarefaction solution, on the isotherm, the flow rapidity is constant. Therefore, the first term is zero, and the second gives simply

$$\frac{1}{\tau_{\text{exp}}} \approx \frac{\sinh(\kappa)}{r}, \quad (26)$$

and is therefore *not* constant over the outer edge region. This agrees with conclusion from analytic 1+1d solution above, for which  $\partial_\mu u^\mu \sim 1/\tau$ , and means that the FOS in the outer edge region needs to be modified.

In the upper plot of Fig. 7 we compare the isotherms with the surfaces obtained from the freezeout condition (Eq. 22). While having qualitatively similar shape, they generally correspond to smaller  $r$  and larger  $\tau$ . The corresponding distribution of the transverse flow rapidity on these surfaces is shown in the lower part of the figure. One can see that improvement of the freezeout condition leads to quite significant enlargements of the “outer edge” plateaus. For example, the curve with  $C = 7$  provides the transverse rapidity  $\kappa \approx 1.4$  (needed for description of the high  $p_\perp$  tail) for larger range of distances, from  $r = 8 \text{ fm}$  to  $r = 27 \text{ fm}$ .

Let us emphasize again, that the improved FOS's depend on the cross section for the particular species. For example, the difference between those for a nucleon and  $\phi$  meson is more than an order of magnitude, and even in the power  $1/P$  they can be as large as 50% difference of  $C_i^{1/P_i}$ , roughly corresponding to the range of parameters shown. If so, in spite of similar mass, the spectra of  $p$  and  $\phi$  at large  $p_\perp$  should be very different, with the “outer edge” component nearly absent in the latter case.

## VIII. EXTENSION TO NON-CENTRAL COLLISIONS

Let us start with the elliptic flow data, for various secondaries, in the same range of transverse momenta as discussed in the previous chapters. In Fig. 8, we have compiled the ALICE data for  $v_2(p_\perp)$  for some secondaries. The general trend is that  $v_2$  *decreases* at  $p_\perp > 3 \text{ GeV}$ , after it reaches a maximum. Before going into details, let us outline a proposed explanation of this trend: the azimuthal asymmetry of the flow is large in the “lid” region, but is very small at the “outer edge”.

We also would like to argue that the “outer edge” FOS and thus flow magnitude is different for different secondaries, while they are much more similar at the “lid”. For this reason we

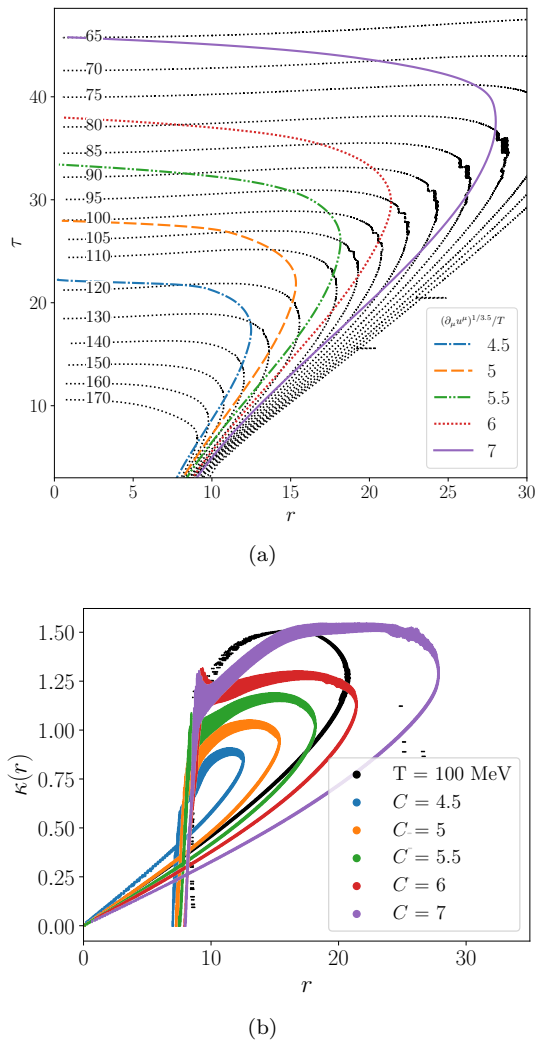


FIG. 7. (a) The isotherms, marked by the dotted lines with the corresponding temperature in MeV, compared with the improved freezeout surfaces corresponding to the condition (22), with the values of the parameter  $C$  indicated on the insert. (b) shows the transverse rapidity  $\kappa(r)$  on the  $T = 100$  MeV isotherm (black) with those corresponding to improved FOS.

included  $v_2$  for  $p$  and  $\phi$ : they are nearly identical below the maximum, at  $p_\perp \approx 2.5$  GeV, dominated by the “lid” region, but are different above it. We remind that these particles have similar mass but very different collision rates with (mostly pion) background matter.

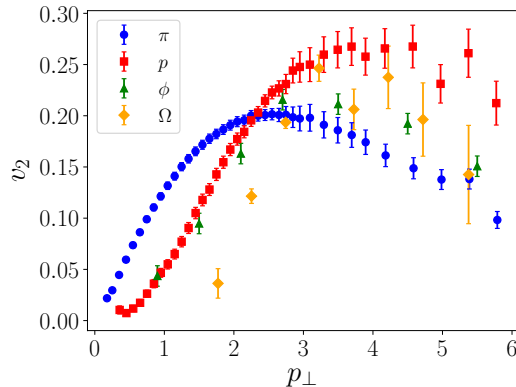


FIG. 8. Elliptic flow parameter  $v_2$  for  $\pi, p, \phi, \Omega$  identified hadrons, shown by blue circles, red squares, green triangles and orange diamonds, respectively. The data are from ALICE collaboration [20], for the centrality bin 20-30%.

To study whether the proposed explanation can be justified from standard hydrodynamical approach, we generated hydro output corresponding to non-central collisions. We use the same centrality bin 20-30% as the data just discussed. For this hydrodynamical solution, we constructed both types of the FOS – the isotherms as well as those corresponding to the freezeout condition (Eq. 22) – and calculated the flow patterns on these surfaces.

In Fig. 9 we show the distributions of the flow rapidity in  $x$  and  $y$  directions, for both types of surfaces. Specifically, to focus on azimuthal asymmetry, we show the distributions over  $u_0 + u_x$  and  $u_0 + u_y$  at the isotherm  $T = 100$  MeV and the improved FOS with  $(\partial_\mu u^\mu)^{1/3.5} = 7T$ . The choice of the quantity is due to the fact that for very ultrarelativistic secondaries, the Boltzmann factor  $\exp(-p^\mu u_\mu/T)$  can be simplified to  $\exp((p/T)(u_0 + u_x))$  when momentum is in the  $x$  direction, and similarly for  $y$  direction. The comparison shows that:

- (i) the improved FOS has more pronounced peaks at the r.h.s. of the plot, the region most important for spectra at large  $p/T$ ;
- (ii) the asymmetry between  $x$  (in the direction of the impact parameter) and  $y$  distributions for the improved FOS is significantly

reduced.

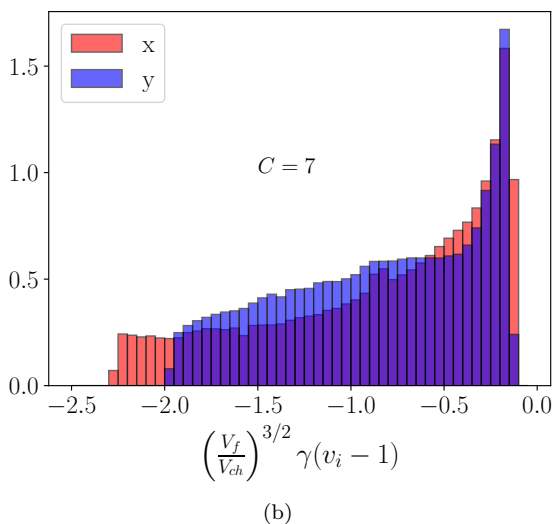
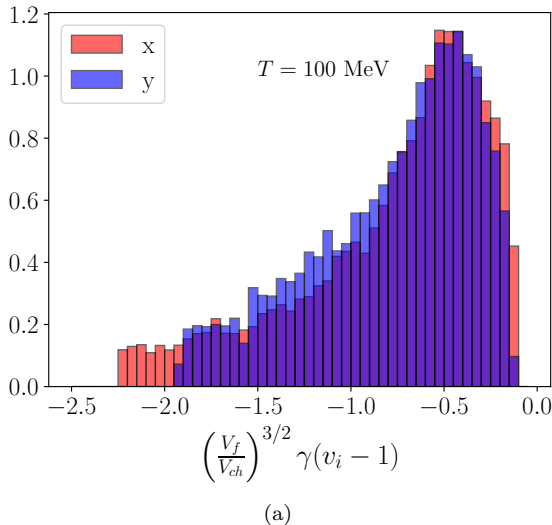


FIG. 9. The distribution over  $u_0 - u_x$  (dark blue) and  $u_0 - u_y$  (light red) on the FOS with (a)  $T = 100$  MeV and (b) the improved surface corresponding to condition Eq. (22) with  $(\partial_\mu u^\mu)^{1/3.5} = 7T$ .

While both these trends are in the direction supporting the proposed explanation of  $v_2(p_\perp)$  behavior, unfortunately quantitatively it still does not work: even the reduced asymmetry at the improved FOS still results in the values of the elliptic flow parameter  $v_2(p_\perp > 2.5 \text{ GeV}) \approx 0.3 - 0.4$ , which is larger than observed. We

also do not observe the marked decrease of  $v_2$  at high  $p_\perp$  observed in the data. We thus conclude that, to better understand particle distributions at the “outer edge” of the fireball, more work is needed.

## IX. SUMMARY AND DISCUSSION

This paper was motivated by two observations. First, the thermal distribution over particle masses correctly describe the data for many orders of magnitude, at least up to the  $M = 4 \text{ GeV}$  of  ${}^4\text{He}$ , and maybe even further. One may also think that thermal exponential distribution in mass implies also thermal exponential distribution in *energy*, in frames co-moving with matter. If so, the experimental spectra can be expressed as a convolution of near-thermal spectrum with appropriate distribution over collective flow velocities.

Our second motivation, coming from spectra themselves, is that their transition to power-like behavior only at  $p_\perp = 5 - 6 \text{ GeV}$ , and below that we see exponential with very smooth growth of “effective temperature.” Its explanation via “blue shift” suggest magnitude of flow compatible with values reached at the “outer edge” of the fireball. Phenomenologically, a simple “lid” plus “outer edge” model does well, reproducing spectra of secondaries with different mass, such as pions and nucleons.

To understand the phenomenon further, we then turn to known analytic solutions. Dismissing Gubser’s solution due to its unphysical behavior at the “outer edge,” we then show that the “rarefaction fan” solution, although 1+1 dimensional, can be used to understand the edge of numerical solutions to hydrodynamics. In particular, a nontrivial feature is that the isotherms and the constant flow rapidity lines are nearly identical.

The next step we took is to use an improved freezeout condition, including not only temperature but also the matter expansion rate defined via  $\partial_\mu u^\mu$ . The corresponding modifications of the FOS are studied, and the flow of magnitude needed to explain the spectra in central collisions is indeed observed on these surfaces.

Turning to non-central collisions we suggest that the observed decrease of  $v_2$  at  $p_\perp >$

2.5 GeV is due to very small azimuthal asymmetry of the flow at the “outer edge”. We found that the improved FOS does indeed have smaller asymmetry than isotherms, but it was still too large to explain the data.

Apparently, more work is needed to understand the conditions at the “outer edge” of the fireball.

Standard hydro-based models use cascade “afterburners,” but since we now discuss tails of the spectra with probabilities down to something like  $10^{-6}$ , this approach is not statistically feasible.

The collision rate corresponding to FOS we use implies large mean free paths of particles at kinetic freezeout about

$$\tau_{\text{coll}} \sim l_{\text{m.f.p.}} \sim 7 \text{ fm}$$

While it may appear large, note that at that stage the fireball is still much larger than this value, with time reaches 30 fm/c and radius about 20 fm. So one does not need to do a cascade of the whole system; rather, a cell of this size should be enough.

We would like to suggest relatively simple modifications of standard hydro may be significant increase of viscosities, bulk and shear, at the late stages. Another can be a substitution of FOS by its “coarse grained” version, on the scale defined by  $l_{\text{m.f.p.}}$ .

Further improvement can involve anisotropic distribution in a cell, in the frame co-moving with the flow. It is clear that isotropic thermal distribution should become anisotropic, given the temperature gradient. Another effect indicated by Ref. [5] is that not only the scalar expansion rate  $\partial_\mu u^\mu$  we used above needs to be included, but the whole tensor of gradients  $\partial_\mu u^\nu$  as well. So far, deformation of the thermal distribution due to it has been only studied when the deformation is small.

#### Appendix A: General expressions for rapidity-independent and axially symmetric flows

Our (relatively standard) assumption is the (longitudinal) *rapidity independence* of flow, and that it is simply equal to spatial rapidity, a la Bjorken. For this case one can integrate the

longitudinal extent of the fireball [1].

$$\frac{dN}{dy dp_\perp^2 d\phi} = \frac{2g_i}{(2\pi)^3} \int d^2 r_\perp \tau_f(r_\perp) e^{\mu/T} e^{(\vec{u}_\perp \vec{p}_\perp)/T} \quad (\text{A1})$$

$$\times [m_\perp K_1(\beta_\perp) - (\vec{p}_\perp \vec{\nabla}_\perp \tau_f) K_0(\beta_\perp)],$$

where  $m_\perp^2 = p_\perp^2 + m^2$ . Since in this work we focus on large momenta, we assume Boltzmann statistics with a single exponent, and the arguments of the Bessel functions  $K_1, K_0$  are the temporal part  $\beta_\perp = m_\perp u_0/T$  of the product of the 4-velocity of the flow

$$u_\mu = \frac{1}{\sqrt{1-v^2}}(-1, \vec{v})$$

to 4-momentum. Note that the temperature  $T$  is not written as a function of the position, since the freezeout surface is usually approximated by the isotherm with constant  $T = T_f$ .

Further simplification is possible when collisions are assumed to be exactly central, with zero impact parameter  $b = 0$ , since the cup is round and analytic integration over azimuthal angle  $\phi$  can be done. The result [1] includes the second set of Bessel functions

$$\frac{dN}{dy dp_\perp^2} = \frac{g_i}{\pi^2} \int dr_\perp r_\perp \tau_f(r_\perp) e^{\mu/T} \quad (\text{A2})$$

$$\times [m_\perp K_1(\beta_\perp) I_0(\alpha_\perp) - p_\perp \left( \frac{\partial \tau_f}{\partial r_\perp} \right) K_0(\beta_\perp) I_1(\alpha_\perp)]$$

with the argument being the 3-d part of the  $u_\mu p^\mu$  product, namely  $\alpha_\perp = (\vec{u} \vec{p}_\perp)/T$ .

#### Appendix B: Implementing nonzero chemical potentials after chemical freezeouts

Ignoring small presence of baryon number at mid-rapidity, one usually assume that before chemical freezeout ( $T_{\text{ch}} \approx 156 \text{ MeV}$ ) all species have zero chemical potential.

However after that, the inelastic collisions are assumed to be absent and the particle numbers of all species are assumed to be conserved. If so, the thermal distributions are appended by *nonzero* chemical potential, whose magnitude is calculated from particle number preservation.

It is approximately given by the following relation

$$e^{\frac{\mu(T)}{T}} = \frac{V_{\text{ch}}}{V_T} \left( \frac{T_{\text{ch}}}{T} \right)^{3/2}. \quad (\text{B1})$$

Since it depends on  $T$  only, it is a constant factor on isotherm FOS. But on the improved FOS's we use the temperature is no longer constant, and thus this fugacity varies at different locations, so it therefore needs to be included in any averaging.

### Appendix C: Hadronic observables in our hydrodynamic calculations

The hadronic observables produced in our hydrodynamic simulations for for 2.76 TeV Pb-Pb collisions with optical Glauber initial conditions and the experimental data are shown in Table I. In general, we have good agreement with data. The  $v_2$  of our calculations is smaller

than that of experiment, which is a well-known result of using optical Glauber initial conditions.

TABLE I. Comparison of calculated and experimental hadronic observables in 2.76 TeV Pb-Pb collisions, for hydrodynamics with bulk viscosity. Experimental data is the same as used in Refs. [21, 22].

	hydro. calc.	data
$N_{\text{pion}}$	309.1	$307 \pm 20$
$\langle p_T   p_T \rangle_{\text{pion}}$	0.508	$0.512 \pm 0.017$
$v_2$	0.0746	$0.0831 \pm 0.0034$

**Acknowledgements** This work was supported by the U.S. Department of Energy under Contract No. DE-FG-88ER40388. We acknowledge help by J.-F. Paquet, who kindly guided us in the use of hydrodynamical numerical solutions generated using the MUSIC code.

- 
- [1] U. W. Heinz, hep-ph/0407360.  
[2] E. Shuryak, Rev. Mod. Phys. **89**, 035001 (2017) doi:10.1103/RevModPhys.89.035001 [arXiv:1412.8393 [hep-ph]].  
[3] R. D. Weller and P. Romatschke, Phys. Lett. B **774**, 351 (2017) doi:10.1016/j.physletb.2017.09.077 [arXiv:1701.07145 [nucl-th]].  
[4] P. Bozek and W. Broniowski, Phys. Rev. C **88**, no. 1, 014903 (2013) doi:10.1103/PhysRevC.88.014903 [arXiv:1304.3044 [nucl-th]].  
[5] D. Teaney and L. Yan, Phys. Rev. C **89**, no. 1, 014901 (2014) doi:10.1103/PhysRevC.89.014901 [arXiv:1304.3753 [nucl-th]].  
[6] R. J. Fries, B. Muller, C. Nonaka and S. A. Bass, Phys. Rev. Lett. **90**, 202303 (2003) doi:10.1103/PhysRevLett.90.202303 [nucl-th/0301087].  
[7] A. Andronic, P. Braun-Munzinger, K. Redlich and J. Stachel, Nature **561**, no. 7723, 321 (2018) doi:10.1038/s41586-018-0491-6 [arXiv:1710.09425 [nucl-th]].  
[8] L. D. Landau, Izv. Akad. Nauk Ser. Fiz. **17**, 51 (1953).  
[9] J. D. Bjorken, Phys. Rev. D **27**, 140 (1983). doi:10.1103/PhysRevD.27.140  
[10] S. S. Gubser, Phys. Rev. D **82**, 085027 (2010) doi:10.1103/PhysRevD.82.085027 [arXiv:1006.0006 [hep-th]].  
[11] S. S. Gubser and A. Yarom, Nucl. Phys. B **846**, 469 (2011) doi:10.1016/j.nuclphysb.2011.01.012 [arXiv:1012.1314 [hep-th]].  
[12] P. Staig and E. Shuryak, Phys. Rev. C **84**, 044912 (2011) doi:10.1103/PhysRevC.84.044912 [arXiv:1105.0676 [nucl-th]].  
[13] E. Shuryak and I. Zahed, Phys. Rev. C **88**, no. 4, 044915 (2013) doi:10.1103/PhysRevC.88.044915 [arXiv:1301.4470 [hep-ph]].  
[14] Y. Hirono and E. Shuryak, Phys. Rev. C **91**, no. 5, 054915 (2015) doi:10.1103/PhysRevC.91.054915 [arXiv:1412.0063 [hep-ph]].  
[15] G. Baym, B. L. Friman, J. P. Blaizot, M. Soyeur and W. Czyz, Nucl. Phys. A **407**, 541 (1983). doi:10.1016/0375-9474(83)90666-8  
[16] B. B. Abelev *et al.* [ALICE Collaboration], Phys. Lett. B **736**, 196 (2014) doi:10.1016/j.physletb.2014.07.011

- [arXiv:1401.1250 [nucl-ex]].
- [17] S. Ryu, S. Jeon, C. Gale, B. Schenke and C. Young, Nucl. Phys. A **904-905**, 389c (2013) doi:10.1016/j.nuclphysa.2013.02.031 [arXiv:1210.4588 [hep-ph]].
- [18] I. Y. Pomeranchuk, Dokl. Akad. Nauk Ser. Fiz. **78**, 889 (1951).
- [19] C. M. Hung and E. V. Shuryak, Phys. Rev. C **57**, 1891 (1998) doi:10.1103/PhysRevC.57.1891 [hep-ph/9709264].
- [20] B. B. Abelev *et al.* [ALICE Collaboration], JHEP **1506**, 190 (2015) doi:10.1007/JHEP06(2015)190 [arXiv:1405.4632 [nucl-ex]].
- [21] S. Ryu, J.-F. Paquet, C. Shen, G. S. Denicol, B. Schenke, S. Jeon and C. Gale, Phys. Rev. Lett. **115**, no. 13, 132301 (2015) doi:10.1103/PhysRevLett.115.132301 [arXiv:1502.01675 [nucl-th]].
- [22] S. Ryu, J. F. Paquet, C. Shen, G. Denicol, B. Schenke, S. Jeon and C. Gale, Phys. Rev. C **97**, no. 3, 034910 (2018) doi:10.1103/PhysRevC.97.034910 [arXiv:1704.04216 [nucl-th]].